Journal of Mechanical Engineering and Sciences
ISSN (Print): 2289-4659; e-ISSN: 2231-8380
Volume 13, Issue 3, pp. 5334-5346, September 2019

DOI: https://doi.org/10.15282/jmes.13.3.2019.09.0435

A two degrees of freedom comb capacitive-type accelerometer with low cross-axis sensitivity

M. N. Nguyen[1,2], L. Q. Nguyen[1], H. M. Chu[1], H. N. Vu[1*]

[1]International Training Institute for Materials Science (ITIMS), Hanoi University of Science and Technology, No1 Dai Co Viet Road, Hai Ba Trung, Hanoi, Vietnam,
*Email: hungvungoc@itims.edu.vn
Phone: +84-24-38680786.
[2]Electrical and Electronic Faculty, Hung Yen University of Technology and Education, Hung Yen Province, Vietnam.

ABSTRACT

In this paper, a SOI-based comb capacitive-type accelerometer sensing acceleration in two lateral directions was designed, fabricated, and experimentally characterized. The structure of the accelerometer was designed using a proof mass connected by four folded-beam springs, which are compliant to inertial displacement caused by attached acceleration in the two lateral directions. At the same time, the folded-beam springs enabled to suppress cross-talk which is caused by mechanical coupling from parasitic vibration modes. The differential capacitor sense structure was employed to eliminate common mode effects. The design of gap between comb fingers was also analyzed to find an optimal sensing comb electrode structure. The design of the accelerometer was carried out using the finite element analysis. The fabrication of the device was based on SOI-micromachining. The characteristics of the accelerometer have been investigated by a fully differential capacitive bridge interface using a sub-fF switched-capacitor integrator circuit. The sensitivities of the accelerometer in the two lateral directions were determined to be 6 and 5.5 fF/g, respectively. The cross-axis sensitivities of the accelerometer were less than 5%, which shows that the accelerometer can be used for measuring precisely acceleration in the two lateral directions. The accelerometer operates linearly in the range of investigated acceleration from 0 to 4g.

Keywords: comb capacitive-type accelerometer, SOI-micromachining, folded-beam spring, cross-axis sensitivity.

INTRODUCTION

Low cost, high performance micromachined accelerometers have attracted research intention for application in daily lives such as air-bag systems in automobiles, measurement of mechanical shock, cell phones and navigation systems [1-3]. There are several sensing mechanisms for detecting acceleration such as piezoresistive, piezoelectric, optical and capacitive [4-12]. The micro machined accelerometers based on capacitive-type sensing mechanism have advantages that consist of high sensitivity, low noise, low temperature sensitivity, and low power consumption [13]. Differential capacitive sensing mechanism has

also been explored to possess high linearity and large signal to noise ratio [14-15]. In order to measure the small capacitance signal in micro machined accelerometers, switched capacitor techniques have been developed [16-18]. Most of reported accelerometers were designed for sensing accelerations in one direction and suppressing other components of the acceleration vector. This kind of device is called uniaxial accelerometer. To meet the need of developing powerful analysis systems, multiple axes accelerometers are prerequisite to develop. The development of MEMS techniques such as bulk and surface micromachining enables to improve substantially the performance and reduce the size of accelerometer. The cost of the device is also decreased due to mass production using MEMS technology. Recently, MEMS accelerometers fabricated on SOI wafer have been attracting intense interest due to the simple and reliable fabrication using buried oxide as an etch stop layer [11, 12]. The out-of-plane z-axis accelerometer with differential capacitive sensing has been developed for integrating monolithically the three-axes accelerometer into SOI wafer [19]. There are also several reports on the two degrees of free accelerometer with differential capacitive sensing [16, 19-21]. However, it is not easy to realize a differential capacitive accelerometer that senses accelerations in two lateral directions. This is because flexible beam structure suspending the proof mass requires a design that is able to provide mobility along two desired sense directions simultaneously. In addition, the mechanical coupling from parasitic vibrations must be suppressed to decrease noise [22].

In this paper, a SOI-based comb capacitive-type accelerometer used for measuring precisely accelerations in two orthogonal lateral directions was designed, fabricated, and experimentally characterized. Folded-beam springs, which are flexible to displacements in the two directions causing by attached acceleration, were used to design the accelerometer. At the same time, the folded-beam springs were also designed to suppress cross-talk caused by mechanical coupling from parasitic vibration modes. The differential capacitor sense structure was used to eliminate common mode effects. The asymmetrical comb electrode structure, i.e., two different capacitance gaps in one pair of comb fingers, was used and optimized to form the differential capacitor sense structure. The design of the accelerometer was carried out with the finite element analysis using ANSYS software. The fabrication of the device was based on SOI-micromachining. The characteristics of the accelerometer have been investigated by a differential capacitive bridge interface using a sub-fF switched-capacitor integrator circuit.

DESIGN

The capacitive-type accelerometer converts the displacement signal into the electrical signal. Figure 1 shows a schematic drawing of the accelerometer. There is a center proof mass that is anchored by four folded-beam springs. The stiffness of folded-beams is designed so that the proof mass can experience displacement in two X and Y directions, which is exerted by the inertial force causing by external acceleration. In addition, the design of folded-beams is also considered to eliminate cross-talk, which causes by mechanical coupling from parasitic vibration modes. The sense comb electrodes are arranged at the outermost edges of the center proof mass. The comb sense capacitance is split into four identical sub-capacitances, C_{r1}, C_{l1}, C_{r2} and C_{l2}, in a symmetrical and differential manner. The sub-capacitances form two pairs of different capacitance in X and Y directions as shown in Figure 1. The asymmetrical comb

electrode structure with two differential capacitance gaps in one pair of comb fingers is used to form the differential capacitor sense structure. When the proof mass displaces, for example, to the right in X direction, the capacitances C_{r2} and C_{l2} will increase and decrease, respectively and inversely. The similar behavior is observed for C_{r1} and C_{l1} in the Y direction. The differential capacitance signal is readout based on sub-fF switched-capacitor integrator circuit (MS3110).

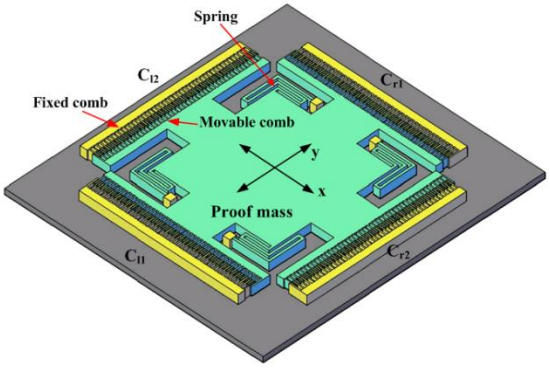

Figure 1. Schematic of two degrees of freedom accelerometer.

As shown in the design model, the principle of differential detection is employed by symmetrically placing capacitive electrodes on two opposing sides of the outermost edges of the proof mass, such that the capacitance change in the electrodes are in opposite directions. It means that a differential capacitive bridge is formed. The change in capacitance for an electrode set with N fingers on each side can be calculated as [23]:

$$\Delta C = 2N\varepsilon_0 \frac{tL}{g^2} Y \tag{1}$$

where t is the thickness of comb finger, L is overlap length, g is the comb gap, Y is the displacement of sensing electrode in the motion direction.

As the initial value of g is 2.5 μm, the limited value for the displacement of the sensing finger is 2 μm. In fact, for the design of sensing capacitive structure as described above, there are two gaps, one of which is a smaller one corresponding to g, the other is larger on the opposite side. In order to optimize the large gap for the arrangement of sensing fingers, several calculations were performed. Fixing a displacement of 1 μm in the sensing motion, a maximum large gap of 7 μm was determined relying on the calculation of the change in capacitance ΔC using Equation (1) as revealed in Figure 2. Despite considering the initial value of small gap, the large one may be between 3 μm and 4 μm. However, the calculated results showed that corresponding to this range the change in the capacitance is small, and even equals to zero if the distance of large gap is 3.5 μm. Subsequently, the total gap between two adjacent fingers on one side of interdigitated capacitor set is 12.5 μm.

In order to have a reasonable capacitance change for detecting applied acceleration, the comb fingers need to be made of a thick device layer. In this study, a SOI wafer with a 30 μm thick device layer is used. Besides, to release the proof mass after Dry Reactive Ion Etching (DRIE), perforated holes are opened for etching buried oxide layer (not shown in Figure 1). The fabrication of perforated holes is also to decrease the slide air film damping between the proof mass and substrate [24]. By changing the dimensions of the spring beams,

the performance of the accelerometer was simulated using the finite element method using an ANSYS software. The designed parameters are chosen for fabrication shown in Table 1.

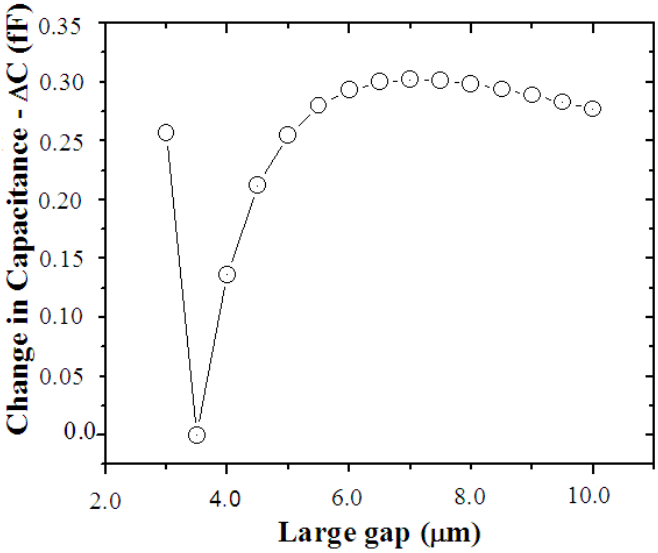

Figure 2. Dependence of capacitance change on large gap.

Table 1. Design parameters of Accelerometer.

Design Parameters	Dimensions/number
Beam width	6 μm
Beam length	236 μm
Mass width	1200 μm
Mass Length	1200 μm
Movable finger width	6 μm
Movable finger length	100 μm
Fixed finger width	6 μm
Fixed finger length	100 μm
Electrode overlap area	90 μm
Total number of fingers	264
Device thickness	30 μm
Anchor size	100 μm x 100 μm
Outermost device area	2000 μm x 2000 μm

Figure 3 shows X- and Y- mode analysis results of the accelerometer. The natural frequencies of X- and Y- mode are 4.583 kHz and 5.065 kHz, respectively. Other analysis results of the vibrating modes correspond to the higher degree modes providing frequencies greater than 7.9 kHz, which are shown in Table 2. Thus, there is a difference of 58% between two first

modes and the higher degree ones. It means that the crosstalk effect can be suppressed [22]. In addition, the sensitivity of the sensor is inversely proportional to the square of natural frequency f_n. Therefore, it is an effective way to increase the sensitivity by decreasing f_n. However, the decrease in f_n, i.e., the suspending spring is soft, makes the proof mass easily stick to the substrate in operation and operation bandwidth decrease due to reducing the natural frequency of the accelerometer. Thus, in order to obtain an accelerometer with desired sensitivity and operation bandwidth, the design parameters of spring beams, dimension of proof mass and sense comb structure must be carefully considered.

Table 2. Four lowest modes of accelerometer.

Mode	Frequency (kHz)
Mode X	4.583
Mode Y	5.065
Rotation mode	7.920
Mode Z	8.606

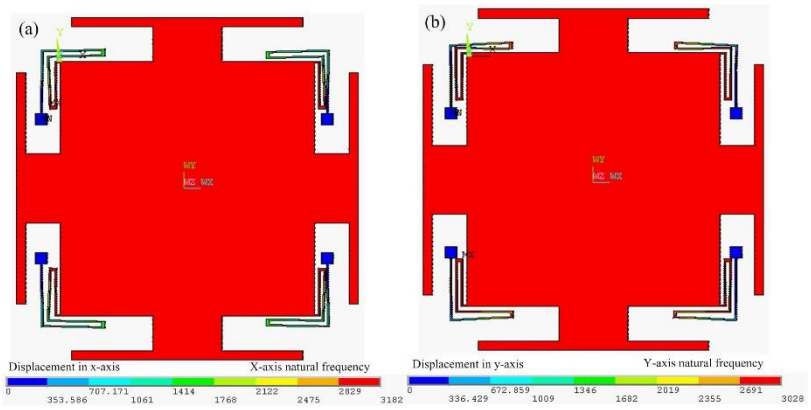

Figure 3. The mode analysis results of accelerometer obtained by ANSYS: (a) X-mode and (b) Y-mode.

FABRICATION

The accelerometer has been fabricated by SOI-based MEMS technology. The main steps in the fabrication process are shown in Figure 4. The 4-inches Silicon-On-Insulator (SOI) wafer was used for fabrication, which has a 30 μm thick top silicon layer, a 4 μm thick buried oxide layer and a 500 μm thick bottom silicon layer (Figure 4 (a)). The SOI wafer has been cleaned by SC process and thermally oxidized to have a protective oxide mask layer in the fabrication of device. First, the structure of sensor including the proof mass, sense combs, springs and holes for post-releasing were patterned by photolithography techniques using a positive photoresist polymer (Figure 4 (b)). The patterned surface was then etched by Deep Reactive Ion Etching (DRIE) to a depth of 30 μm to reach the buried dioxide layer of SOI wafer (Figure (c)). Vapour HF etching process was carried out to etch the SiO_2 layer underneath

the device layer and release the movable electrodes, beams and proof mass (Figure 4 (d)). The SOI wafer was then diced to separate each sensor.

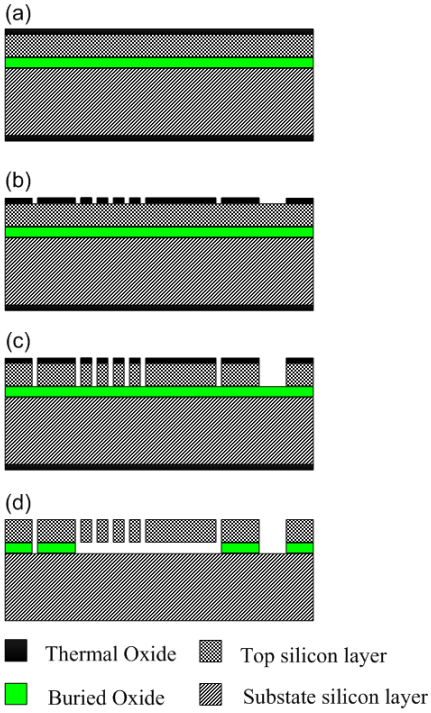

Figure 4. Fabrication process of accelerometer.

Packaging was the final step to complete the fabricated sensors. Firstly, the sensor chip was bonded on a device holder using two components epoxy, which is made of hard plastic with pins for use. Wire bonding process was carried out in the next step. In this step, the Westbond 7400C was used for wire bonding. When the fabrication period was finished, the characteristics of sensors were investigated by self-built measurement system using a sub-fF switched-capacitor integrator circuit (MS3110).

EXPERIMENTAL MEASUREMENT

The block diagram of the measurement system used for investigating the acceleration sensor is shown in Figure 5. The measurement system is composed of an interface electronic circuit, analogue to digital converter, a parallel port and a control computer. The interface electronic circuit is a switched-capacitor integrator circuit, which consists of a charge amplifier, low-pass filter, and a buffer for amplification. It outputs a voltage that is proportional to the change in capacitance. C_{st1} and C_{st2} are the internal trimming capacitances that can be adjusted to balance the external capacitances, C_{s1} and C_{s2}. The differential capacitor pair of the acceleration sensor are connected as C_{s1} and C_{s2}, and the internal trimming capacitances C_{st1} and C_{st2} are used to balance the circuit, that is to eliminate any offset in the baseline of

the voltage output. The two pairs of capacitors, C_{r1} and C_{l1} and C_{l2} and C_{r2} in Figure 1, represent for C_{st1} and C_{st2}, respectively.

When an external acceleration applies on the sensor, the capacitances of C_{s1} and C_{s2} are changed; these are reflected as the output voltage, as the bridge is no longer balanced. Charge amplifiers are used in read-out circuitry as they have the advantage of measuring very small charges thus enabling small capacitance measurement. A charge amplifier consists of an operational amplifier with a feedback capacitor (C_F). The feedback capacitor has a wide range of values for selection and the selected value determines the sensitivity of the measurement. The charge amplifier is followed by a low pass filter (LPF), which filters out the high frequency components of the signal; noise tends to be of high frequency. The maximum frequency response of the circuit is limited by the LPF, the break-frequency of which is adjustable from 500 Hz to 8 kHz. The final stage is the amplification of the signal using buffering components and amplifiers. The signal from the output buffer is converted to digital mode using an analogue to digital (A/D) converter on a National Instruments data acquisition board controlled via LabView software. The circuit is placed in the socket of the evaluation board and it is interfaced to the computer via a parallel port (NI USB – 6009).

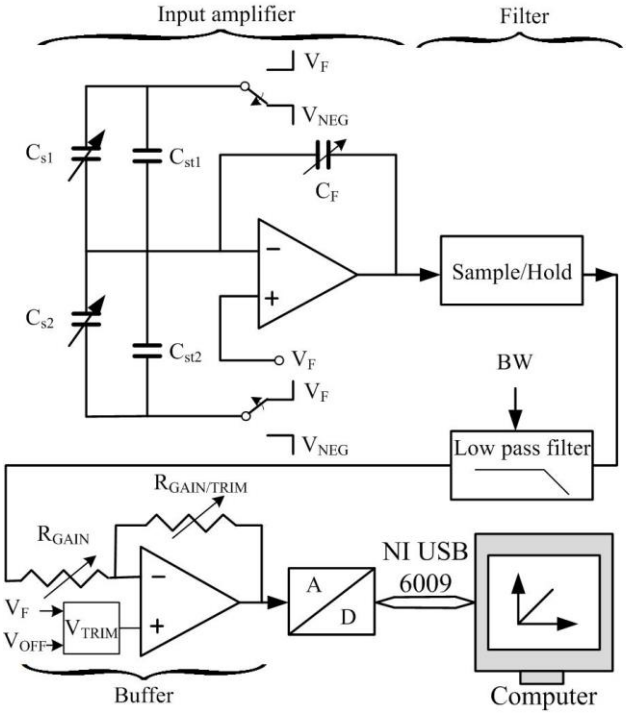

Figure 5. Block diagram of measurement system.

In order to investigate the operation characteristics, the fabricated accelerometer is electrically connected to the circuit on the evaluation board. This sensor system is fixed on a vibration table. The external accelerometer is generated using the vibrator, which can be controlled by a function generator to change the amplitude and/or the frequency of vibration. The acceleration that the vibrator can generate is ± 4g. The generated acceleration is based on the following principle. The sensor displacement can be formulated by the equation:

$$x = A\sin(\omega t + \varphi) \tag{2}$$

where, A is amplitude, ω angular frequency, φ initial phase. The acceleration of the vibration is defined by the second order differential equation of motion:

$$a = \frac{d^2x}{dt^2} = -A\omega^2 \sin(\omega t + \varphi) \tag{3}$$

In Equation (3), $-A\omega^2$ is the amplitude of vibrating acceleration. The acceleration values can be adjusted by the control of input amplitude or frequency. Figure 6 shows the picture of the setup measurement system. Here, in order to calibrate generating acceleration, a standard accelerometer (AVT-CZ Mitutoyo) was used.

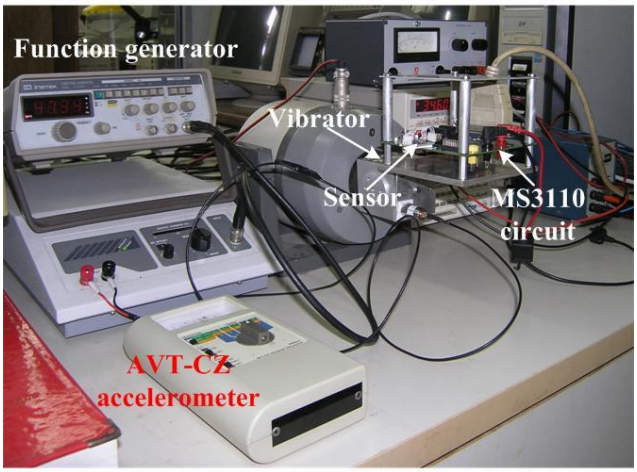

Figure 6. Vibration system for investigating the characteristics of accelerometer.

RESULTS AND DISCUSSION

The accelerometer was fabricated successfully by the proposed processes. The fabricated accelerometer was characterized by a scanning electron microscope (SEM). Figure 7 is the SEM micrographs of fabricated accelerometer with top view (Figure 7 (a)), magnified image of spring and perforated holes for post-releasing (Figure 7 (b)), and magnified image of sense comb fingers (Figure 7 (c)). The comb fingers have well-defined rectangular shapes. The operation testing of fabricated devices has been performed on every wafer. The fabrication yield of the accelerometer is higher than 80%.

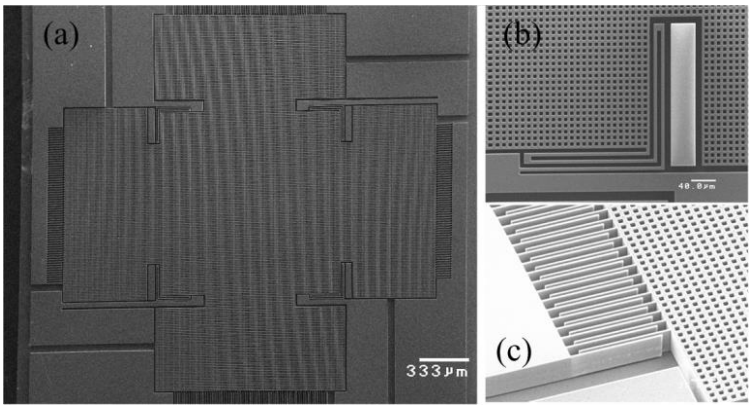

Figure 7. SEM micrographs of fabricated accelerometer: (a) top view, (b) magnified image of spring and perforated holes for post-releasing and (c) magnified image of sense comb fingers.

Figure 8 shows a picture of an array of six accelerometers bonded on a circuit board. The aluminium wiring was well carried out for the electrodes located in the corners.

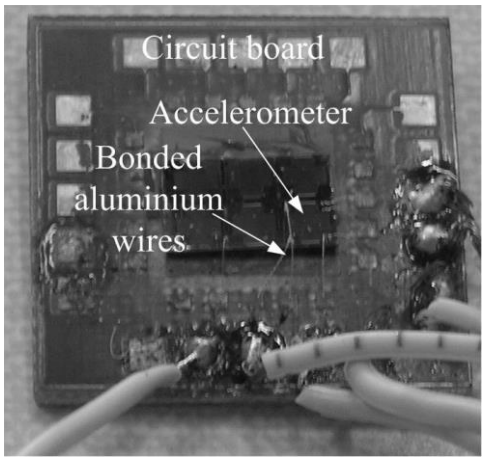

Figure 8. A six-accelerometer array bonded on a circuit board for investigating characteristics.

Figure 9 (a) and (b) show the frequency responses of fabricated 2-DOF comb capacitive-type accelerometers. The measured resonance frequencies are 5.325 kHz and 5.850 Hz for the X and Y directions, respectively. This result has a small difference compared to that of simulation. This is because during the fabrication process, many holes have been drilled on the proof mass of the sensor that causes the mass of sensor's proof mass to decrease. Therefore, the resonance frequencies increase from 4.583 kHz to 5.325 kHz and 5.065 kHz to 5.850 kHz for the X and Y directions, respectively.

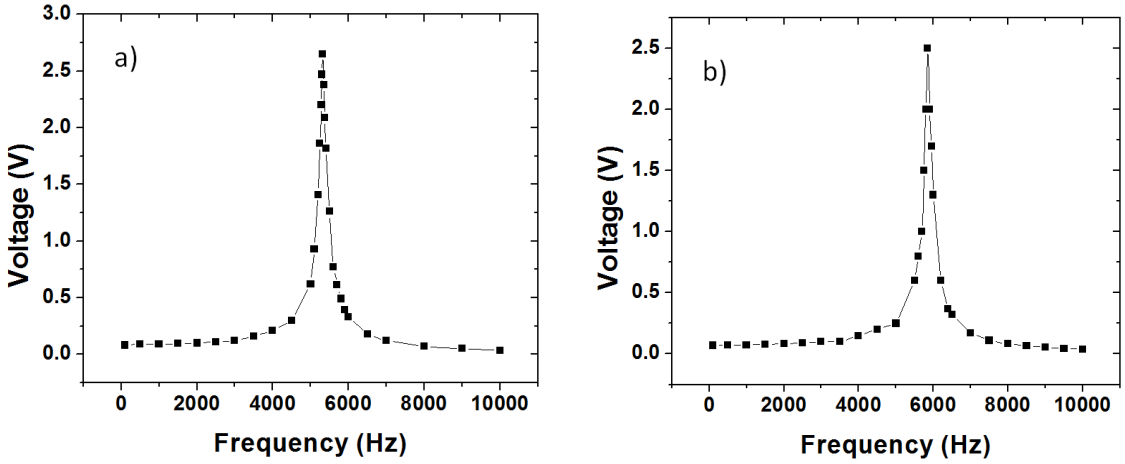

Figure 9. Frequency response of accelerometer: (a) X mode and (b) Y mode.

Figure 10 and Figure 11 show the output characteristics of the accelerometer for the X and Y directions, respectively. The sensitivities of the sensor system were obtained to be 13 mV/g and 11 mV/g, which correspond to the sensitivities of the sensor itself to be 6 fF/g and 5.5 fF/g for the X and Y directions, respectively.

The cross-axis sensitivities of the sensor were also investigated using the vibration table system. Figure 10 and Figure 11 provide the investigated results of cross-sensitivity when applying acceleration for the X direction and for the Y direction, respectively. The investigated results show that the cross-axis sensitivity of the system is about 4.5% for the X direction and 5% for the Y direction. It can be concluded that the accelerometer meets application specifications [25].

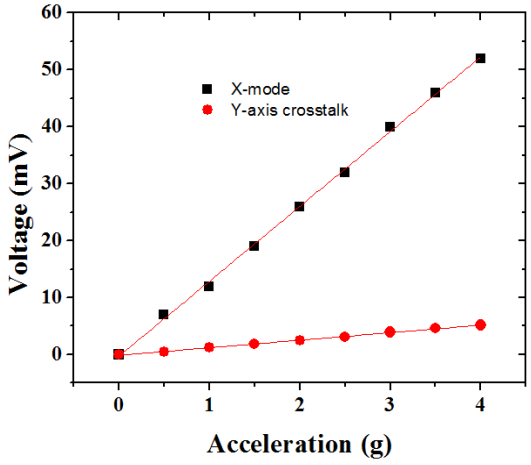

Figure 10. Output voltage and cross-sensitivity of the accelerometer measured as a function of applied acceleration in X direction.

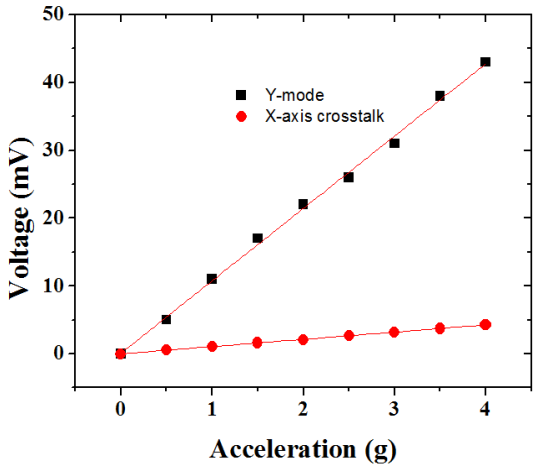

Figure 11. Output voltage and cross-sensitivity of the accelerometer measured as a function of applied acceleration in Y direction.

CONCLUSION

The design, fabrication, and characteristics of a two degrees of freedom SOI-based comb capacitive-type accelerometer have been presented. The structure of the accelerometer was designed using a proof-mass connected by four folded-beam springs that are compliant to inertial displacement causing by attached acceleration in the two lateral directions. The design of the folded-beam springs also suppressed cross-talk causing by mechanical coupling from parasitic vibration modes. The design was carried out using the finite element analysis. The fabrication of the device was based on SOI-micromachining. The characteristics of the accelerometer have been investigated by a fully differential capacitive bridge interface. The sensitivities of the accelerometer in the two lateral directions were determined to be 6 fF/g and 5.5 fF/g, respectively. The cross-axis sensitivities of the accelerometer were less than 5%, which shows that the accelerometer can be used for measuring precisely acceleration in the two lateral directions. The accelerometer operates linearly in the range of investigated acceleration from 0 to 4g.

ACKNOWLEDGEMENTS

This work is supported by the Ministry of Science and Technology (MOST), Vietnam under the NAFOSTED project coded MS 103.99-2014.34.

REFERENCES

[1] Chau KHL, Lewis SR, Zhao Y, Howe RT, Bart SF, Marcheselli RG. An integrated force-balanced capacitive accelerometer for low-g applications. Sensors and Actuatuator A: Physical. 1996; 54: 472-476.

[2] Dong J, Li X, Wang Y, Lu D, Ahat S. Silicon micromachined shock accelerometers with a curved-surface-application structure for over-range stop protection and free-mode-resonance depression. Journal of Micromechanics and Microengineering. 2002; 12: 742-746.

[3] Bouten CVC, Koekkoek KTM, Verduin M, Kodde L, Janssen JD. A triaxial accelerometer and portable data processing unit for the assessment of daily physical activity. IEEE Transactions on Biomedical Engineering. 1997; 44(3): 136-147.

[4] Roy AL, Bhattacharyya TK. Design, fabrication and characterization of high performance SOI MEMS piezoresistive accelerometers. Microsystem Technologies. 2015; 21(1): 55-63.

[5] Tian B, Liu H, Yang N, Zhao Y, Jiang Z. Design of a Piezoelectric Accelerometer with High Sensitivity and Low Transverse Effect. Sensors. 2016; 16(10): 1587-1593.

[6] Chu CL, Lin CH, Fan KC. Two-dimensional optical accelerometer based on commercial DVD pick-up head. Measurement Science and Technology. 2007; 18: 265-274.

[7] Antunes P, Varum H, André P. Uniaxial fiber Bragg grating accelerometer system with temperature and cross axis insensitivity. Measurement. 2011; 44: 55-59.

[8] Kumar KS, Swamy KBM, Mukherjee B, Sen S. Testing of MEMS capacitive accelerometer structure through electro-static actuation. Microsystem Technologies. 2013; 19: 79-87.

[9] Aaltonen L, Halonen K. Continuous-time interface for a micromachined capacitive accelerometer with NEA of 4 μg and bandwidth of 300 Hz. Sensors and Actuatuator A: Physical. 2009; 154(1): 46-56.

[10] Linxi D, Yongjie L, Haixia Y, Lingling S. Characteristics of a novel biaxial capacitive MEMS accelerometer. Journal of Semiconductor. 2010; 31(5): 054006.

[11] Mistry KK, Swamy KBM, Sen S. Design of an SOI-MEMS high resolution capacitive type single axis accelerometer. Microsystem Technologies. 2010; 16: 2057-66.

[12] Zou X, Che L, Wu J, Li X, Wang Y. A novel sandwich capacitive accelerometer with a symmetrical structure fabricated from a D-SOI wafer. Journal of Micromechanics and Microengineering. 2012; 22(8): 085031.

[13] Yubin J, Yilong H, Rong Z. Bulk silicon resonant accelerometer. Chinese Journal of Semiconductors. 2005; 26 (2): 281-286.

[14] Kumar KS, Chatterjee P, Mukherjee B, Swamy KBM, Sen S. A Differential Output Interfacing ASIC for Integrated Capacitive Sensors. IEEE Transactions on Instrumentation and Measurement. 2018; 67(1): 196-203.

[15] Tirupathi R, Kumar KS. A Differential Output Switched Capacitor based Capacitive Sensor Interfacing Circuit. IEEE TENCON 2018: 2018 IEEE Region 10 Conference. 2018; 0565-0569.

[16] Amini BV, Abdolvand R, Ayazi F. A 4.5-mW Closed-Loop ∑Δ Micro-Gravity CMOS SOI Accelerometer. IEEE Journal of Solid-State Circuits. 2006; 41: 2983-2991.

[17] Zhou X, Che L, Wu J, Li X, Wang Y. A novel sandwich capacitive accelerometer with a symmetrical structure fabricated from a D-SOI wafer. Journal of Micromechanics and Microengineering. 2012; 22(8): 085031.
[18] Tseng SH, Lu MSC, Wu PC, Teng YC, Tsai HH, Juang YZ. Implementation of a monolithic capacitive accelerometer in a wafer-level 0.18 μm CMOS MEMS process. Journal of Micromechanics and Microengineering. 2012; 22(5): 055010.
[19] Matsumoto Y, Nishimura M, Matsuura M, Ishida M. Three-axis SOI capacitive accelerometer with PLL C-V converter. Sensors and Actuatuator A: Physical. 1999; 75: 77-85.
[20] Lee JS, Lee SS. An isotropic suspension system for a biaxial accelerometer using electroplated thick metal with a HAR SU-8 mold. Journal of Micromechanics and Microengineering. 2008; 18(2): 025036.
[21] Xie J, Agarwal R., Liu Y, Tsai JM, Ranganathan N. Compact electrode design for an in-plane accelerometer on SOI with refilled isolation trench. Proceeding Transducers' 11. 2011; 76.
[22] Weinberg MS, Kourepenis A. Error sources in in-plane silicon tuningfork MEMS gyroscopes. Journal of Micromechanics and Microengineering. 2006; 15: 479-491.
[23] Madou MJ. Fundamentals of Microfabrication, CRC Press, Boca Raton, FL.1997; 145-160 and 464-468.
[24] Zhang X, Tang WC. Viscous air damping in laterally driven microresonators. Proceeding IEEE MEMS. 1994; 199-204.
[25] Jono K, Hashimoto M, Esashi M. Electrostatic servo system for multi-axis accelerometers. Proceeding IEEE MEMS. 1994; 251-256.